PHYSICAL REVIEW B **74**, 020404(R) (2006)

Bandwidth-disorder phase diagram of half-doped layered manganites

R. Mathieu,[1,*] M. Uchida,[1] Y. Kaneko,[1] J. P. He,[1] X. Z. Yu,[1] R. Kumai,[2] T. Arima,[1,3] Y. Tomioka,[2] A. Asamitsu,[1,4] Y. Matsui,[1,5] and Y. Tokura[1,2,6]

[1]*Spin Superstructure Project (ERATO-SSS), JST, AIST Central 4, Tsukuba 305-8562, Japan*

[2]*Correlated Electron Research Center (CERC), AIST Central 4, Tsukuba 305-8562, Japan*

[3]*Institute of Multidisciplinary Research for Advanced Materials, Tohoku University, Sendai 980-8577, Japan*

[4]*Cryogenic Research Center (CRC), University of Tokyo, Bunkyo-ku, Tokyo 113-0032, Japan*

[5]*Advanced Materials Laboratory, National Institute for Materials Science (NIMS), Tsukuba 305-0044, Japan*

[6]*Department of Applied Physics, University of Tokyo, Tokyo 113-8656, Japan*

(Received 28 June 2006; published 27 July 2006)

Phase diagrams in the plane of r_A (the average ionic radius, related to the one-electron bandwidth W) and σ^2 (the ionic radius variance, measuring the quenched disorder), or bandwidth-disorder phase diagrams, have been established for perovskite manganites, with a three-dimensional (3D) Mn-O network. Here we establish the intrinsic bandwidth-disorder phase diagram of half-doped layered manganites with a two-dimensional (2D) Mn-O network, examining in detail the parent state of the colossal magnetoresistance phenomenon in crystals without ferromagnetic instability. The consequences of the reduced dimensionality, from 3D to 2D, for the order-disorder phenomena in the charge-orbital sectors are also highlighted.

DOI: 10.1103/PhysRevB.74.020404 PACS number(s): 75.47.−m, 71.27.+a

Half-doped perovskite manganites with small bandwidth W and small amount of disorder like $Pr_{0.5}Ca_{0.5}MnO_3$ (Pr^{3+} and Ca^{2+} being small and similar in size) exhibit a long-range charge and orbital order[1,2] (CO-OO). This CO-OO, which is associated with the spin ordering (the so-called CE-type structure[3]), is schematically illustrated in the top left panel of Fig. 1. As for the spin sector, the structure is essentially composed of ferromagnetic zigzag chains antiferromagnetically coupled to one another. A fragment of such a zigzag chain is highlighted in the figure. If the disorder becomes larger due to the ion size mismatch of R^{3+} and A^{2+}, as in $Gd_{0.5}Sr_{0.5}MnO_3$ or $Eu_{0.5}Ba_{0.5}MnO_3$, only the short-range CO-OO order is observed,[2,4] producing a CE-glass state.[4–6] Interestingly, the colossal magnetoresistance effect was found to arise from within this coarse-grained homogeneous CE-glass state.[6,7] In layered systems, the MnO_2 planes (ab planes) are isolated by two blocking $(R/A)O$ layers, so that the CO-OO correlation is limited by the two-dimensional (2D) character of the Mn network. Yet $La_{0.5}Sr_{1.5}MnO_4$ is a well-known half-doped single-layered manganite with concomitant charge and orbital ordering[8] near 220 K. The spin sector orders antiferromagnetically (AFM) at $T_N=110$ K.[8] Akin to the perovskite case, crystals with smaller bandwidth such as $Pr_{0.5}Ca_{1.5}MnO_4$ (PCMO) show CO-OO transitions above room temperature.[9] However, no other half-doped R-Sr-Mn-O system seems to exhibit a long-range CO-OO. A CE-glass state is observed in crystals with larger quenched disorder, such as $Eu_{0.5}Sr_{1.5}MnO_4$ (Eu^{3+} is smaller than La^{3+}, which is already smaller than Sr^{2+}).[10] In the present Rapid Communication, using high-quality single crystals of $R_{0.5}A_{1.5}MnO_4$ manganites, we investigate the CE-glass state and its location in the plane of quenched disorder vs bandwidth. The quenched disorder associated with the solid solution of the A-site cations[4] is quantified using the ionic radius variance $\sigma^2=\Sigma_i x_i r_i^2-r_A^2$, according to the scheme devised by Attfield.[11] x_i and r_i are the fractional occupancies ($\Sigma_i x_i=1$) and electronic radii of the different i cations on the A site, respectively, and $r_A=\Sigma_i x_i r_i$ represents the average A-site ionic radius, related to the bandwidth.

High-quality single crystals of the A-site disordered $R_{0.5}Ca_{1.5}MnO_4$ (RCMO), $R_{0.5}Sr_{1.5}MnO_4$ (RSMO), and $R_{0.5}(Ca_{1-y}Sr_y)_{1.5}MnO_4$ (RCSMO) manganites were grown by the floating zone method [R=La, $La_{1-y}Pr_y$, Pr, Nd, $La_{0.5}Eu_{0.5}$ (~Nd), Sm, or Eu, while A=Ca, or $Ca_{1-y}Sr_y$]. The phase purity of the crystals was checked by x-ray diffraction and the cation concentrations of some of the crystals were confirmed by inductively coupled plasma spectroscopy. The ac susceptibility $\chi(\omega=2\pi f)$ data were recorded as a function of the temperature T and frequency f on an MPMSXL superconducting quantum interference device magnetometer equipped with the ultra-low-field option (low frequencies) and a PPMS6000 (higher frequencies) from Quantum Design, after carefully zeroing or compensating the background magnetic fields of the systems. The resistivity ρ of the crystals was measured using a standard four-probe method on a PPMS6000, feeding the electrical current in the ab plane. The single-crystal x-ray data were recorded at 370 K on a Rigaku SPD curved imaging plate system at the beamline BL-1A of the Photon Factory, KEK, Japan. Thin specimens were prepared for observation with transmission electron microscope by Ar^+ ion milling at low temperatures, to perform the electron diffraction (ED) measurements, and collect the selected-area electron diffraction patterns (EDPs) and dark-field (DF) images. The structural modulation wave vector $q=a^*[\delta\ \delta\ 0]$ (a is the lattice constant, $aa^*=1$) was determined at different temperatures.

$Eu_{0.5}Ca_{1.5}MnO_4$ (ECMO) is very similar to PCMO, albeit with a larger variance ($\sigma^2\sim 7\times 10^{-4}$ Å^2 instead of $\sim 2\times 10^{-7}$ Å^2 for PCMO). The CO-OO remains long ranged in all the RCMO crystals, even when a small amount of Ca is substituted with Sr. For example, in the insets of Fig. 1, we show the [001] zone-axis electron diffraction patterns of $Eu_{0.5}(Ca_{1-y}Sr_y)_{1.5}MnO_4$ (ECSMO) obtained at 80 K. In addition to the fundamental spots (associated with the K_2NiF_4

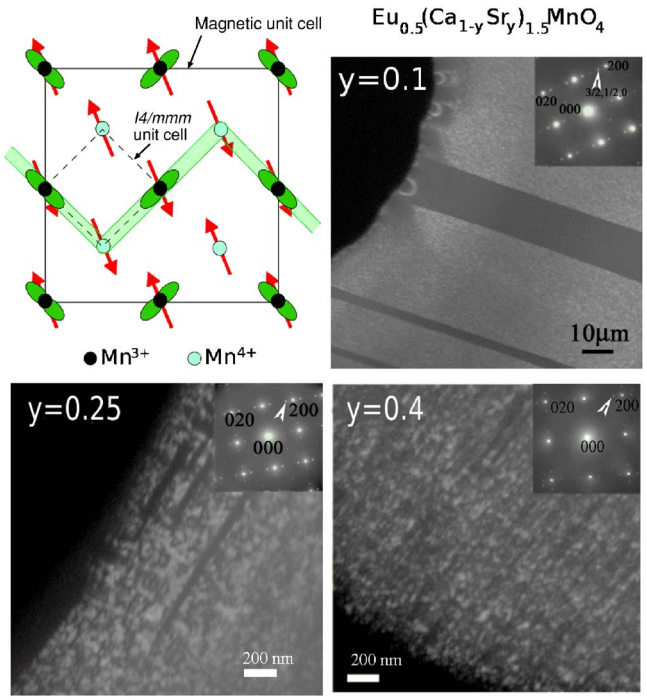

FIG. 1. (Color online) Dark-field images of $Eu_{0.5}(Ca_{1-y}Sr_y)_{1.5}MnO_4$, illustrating the long-range CO-OO order for $y=0.1$ and 0.25 and the short-range CO-OO state for $y=0.4$; $T=80$ K. The corresponding electron diffraction patterns, indexed based on a tetragonal cell with $a\sim3.8$ Å and $c\sim12.4$ Å for simplicity, are shown on the right top corners of the respective panels. A schematic view of the CE-type structure in the basal plane of the tetragonal structure is also depicted. The orbital order involves staggered $3x^2-r^2$ and $3y^2-r^2$ orbitals of the e_g-like electrons of Mn^{3+}, represented as green (dark gray) lobes in the figure. The spins, represented with red (dark gray) arrows, order ferromagnetically along zigzag chains, a fragment of which is highlighted in light green (light gray) in the figure.

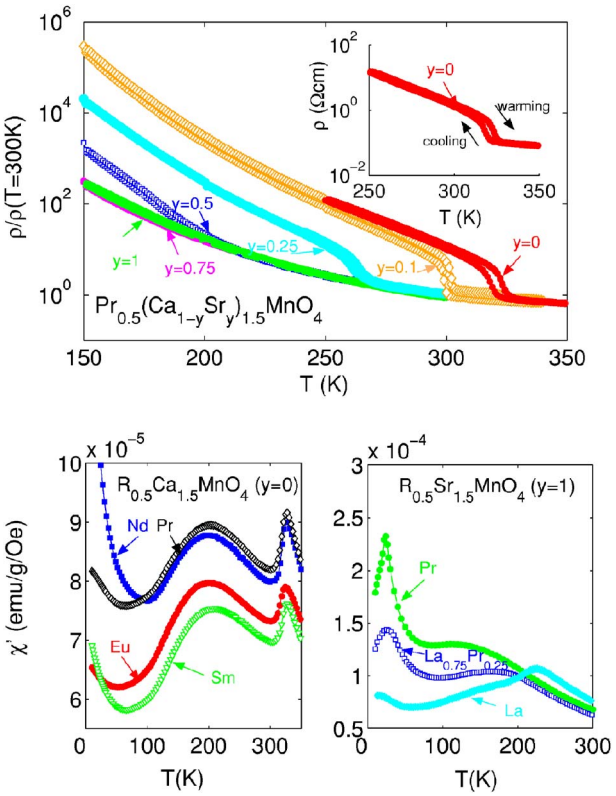

FIG. 2. (Color online) Top panel: Temperature T dependence of the normalized in-plane resistivity $\rho/\rho_{(T=300\ \mathrm{K})}$ for $Pr_{0.5}(Ca_{1-y}Sr_y)_{1.5}MnO_4$. The inset shows the resistivity ρ of the crystal with $y=0$ (PCMO) in absolute units. Lower panel: Temperature dependence of the in-plane component of the ac susceptibility χ' for some of the (left) $R_{0.5}Ca_{1.5}MnO_4$ and (right) $R_{0.5}Sr_{1.5}MnO_4$ crystals. The low-temperature upturn of $\chi'(T)$ in the *R*CMO crystals is attributed to the $4f$ moments of the R cations.

structure), the EDPs include superlattice (SL) spots, associated with the CO-OO. The sharpness and the modulation wave vector, however, are dependent on the Sr concentration (see below). The different panels of Fig. 1 illustrate the changes in the microstructure related to the CO-OO with increasing Sr content. These dark-field images were recorded at 80 K, using the SL reflection marked by the arrow in the electron diffraction patterns. The bright regions in Fig. 1 correspond to regions where the CO-OO occurs. For $y=0.1$ large CO-OO domains are observed. On increasing Sr content, the size of the CO-OO domains decreases ($y=0.25$), until the CO-OO becomes short ranged ($y=0.4$).

The order-disorder in the charge-orbital sector also affects macroscopic properties such as the magnetization or ac susceptibility, as well as the electrical resistivity. For example, the disappearance of the long-range CO-OO state is observed in the T dependence of the electrical resistivity, as shown in the upper panel of Fig. 2 for $Pr_{0.5}(Ca_{1-y}Sr_y)_{1.5}MnO_4$ (PCSMO). The $\rho(T)$ curves show a clear (and hysteretic in temperature) inflection near the CO-OO transition temperature $T_{\mathrm{CO\text{-}OO}}$ up to $y=0.5$, for which no CO-OO phase transition occurs, as confirmed by the ED data. $T_{\mathrm{CO\text{-}OO}}$ is also clearly observed in the $\chi(T)$ curves as the sharp peak arising from the quenching of the FM spin fluctuation. Figure 2 shows the temperature dependence of the in-phase component of the ac susceptibility χ' for some of the single crystals. T_N is however difficult to identify, as seen for example in the $\chi(T)$ curves of the well-known LSMO.[12] As seen in the left lower panel of Fig. 2, in the *R*CMO crystals with small disorder ($\sigma^2<1\times10^3$ Å^2) and relatively small average ionic radius ($r_A\sim1.16$–1.18 Å), a sharp peak marking $T_{\mathrm{CO\text{-}OO}}$ is observed above 320 K. At lower temperatures, near 200 K, a broader peak is observed. This broader peak does not correspond to T_N for long-range spin order, which is ~120–130 K in these crystals.[13] An inflection [more clearly seen in the T derivative of $\chi'(T)$] can been seen in the vicinity of these temperatures, which was found to coincide with the T_N determined by diffraction techniques.[13] The broad maximum near 200 K may thus indicate the development of in-plane AFM correlation, rather than the long-ranged phase AFM transition. We refer in the following to this broad peak as $T_S^*(ab)$. In the *R*SMO crystals, with larger $r_A(\sim1.28$ Å) and bandwidth, only the susceptibility of LSMO (the right lower panel of Fig. 2) shows the $T_{\mathrm{CO\text{-}OO}}$ peak, as well as a bump near 150 K which may reflect the above-mentioned in-plane spin correlation. As the variance (quenched disor-

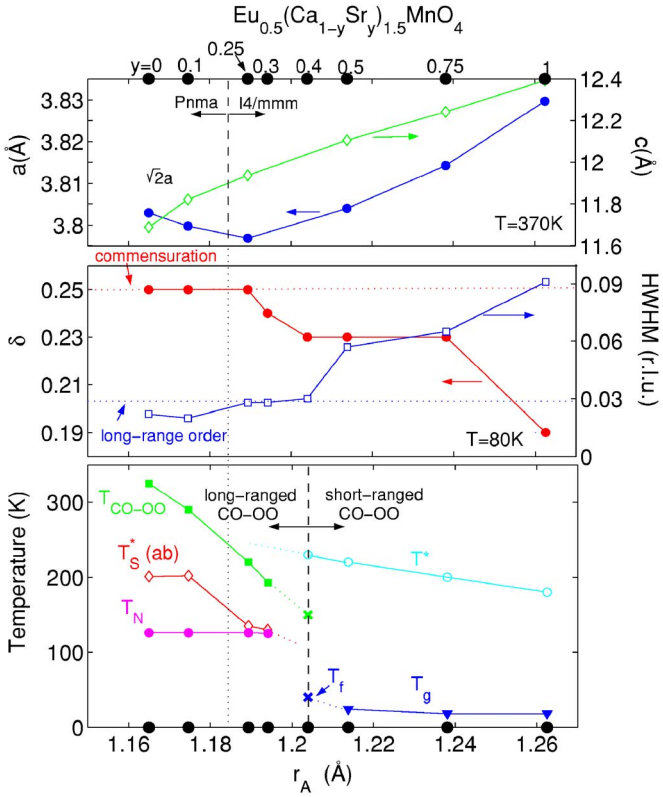

FIG. 3. (Color online) Average ionic radius r_A dependence of selected physical properties of $Eu_{0.5}(Ca_{1-y}Sr_y)_{1.5}MnO_4$. Top: a- and c-axis lattice parameters; $a \sim b$ for the crystals with *Pnma* structure. Middle: Modulation wave vector δ and half width at half maximum (HWHM) of the superlattice reflection intensity profile obtained from electron diffraction at $T=80$ K. Bottom: the electronic phase diagram of $Eu_{0.5}(Ca_{1-y}Sr_y)_{1.5}MnO_4$ (see text for the definitions of the different labels). The crosses mark features in $\rho(T)$ or $\chi(T)$ curves, which do not necessarily correspond to phase transitions.

der) increases with substitution of the La ions with Pr, only a broad peak is observed at high temperatures, together with a broad frequency-dependent cusp at low temperatures.[14] We now compare these observations with the electron diffraction data. In the EDPs collected as a function of temperature, the superlattice spots associated with the CO-OO are observed for all the *R*SMO crystals (one such spot is marked with an arrow in the EDP of ECMO shown in the corner of the top left panel of Fig. 1). However, these SL spots are sharp only for LSMO, and diffusive, more or less, for the crystals with larger R, confirming the short-ranged nature of the CO-OO correlation[15] as suggested by the absence of a sharp peak in $\chi(T)$. Thus in the half-doped case, the orbital sector, as the master, controls the spin sector, as the slave, determining the spatial extent of its correlation as well.

The distinction between long-range and short-range CO-OO is investigated in more detail, as a function of the bandwidth (r_A, or the Sr concentration y) in Fig. 3. The top panel of Fig. 3 shows the variation of the lattice parameters of ECSMO, estimated at high temperatures ($>T_{CO\text{-}OO}$) from single-crystal x-ray diffraction. The a- and c-axis parameters decrease significantly with decreasing y, down to $y=0.25$. These crystals have a tetragonal $I4/mmm$ structure similar to

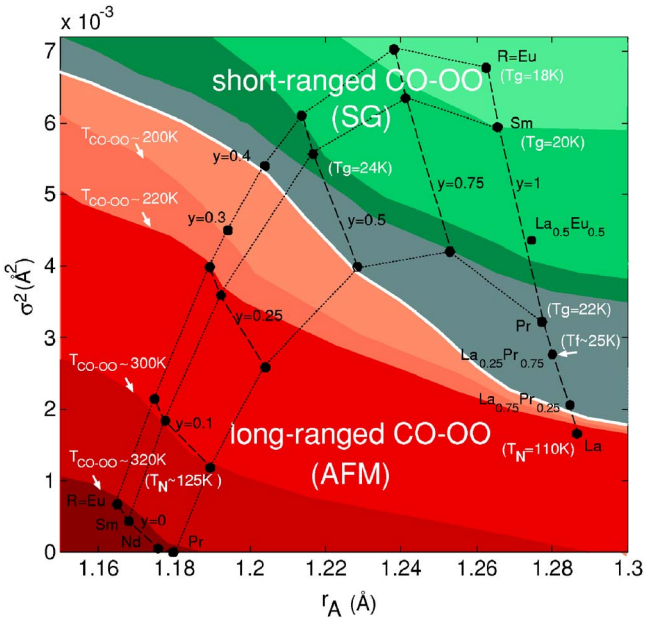

FIG. 4. (Color online) Electronic phase diagram of $R_{0.5}(Ca_{1-y}Sr_y)_{1.5}MnO_4$ in the plane of the average ionic radius r_A and the variance σ^2. Dashed lines connect the crystals with the same Sr content y, while dotted line connect crystals with the same R cation. Data of the CO-OO (the CO-OO transition temperature $T_{CO\text{-}OO}$) and magnetic [the spin-glass (SG) phase transition temperature T_g, the freezing temperature T_f, and the antiferromagnetic (AFM) transition temperature T_N, in parentheses] are included.

that of the *R*SMO crystals. For $y<0.25$, the structure is orthorhombically distorted.[16] However, this structural transition does not coincide with the appearance of the long-range CO-OO order. The $\chi(T)$ and $\rho(T)$ curves suggest that the CO-OO order becomes short ranged near $y=0.4$. This is confirmed by the ED data, as illustrated in the middle panel of Fig. 3. The half width at half maximum (HWHM) of the CO-OO superlattice spots in the EDPs is proportional to the inverse of the CO-OO correlation length $\xi_{CO\text{-}OO}$. In the case of $y=0.4$, the HWHM is relatively small; however, dark-field imaging reveal the short-ranged nature of the CO-OO order (cf. Fig. 1). As y increases above 0.4, the HWHM gradually increases, i.e., $\xi_{CO\text{-}OO}$ gradually decreases, down to the nanometer scale.[10] The modulation wave vector of the SL spots also varies with r_A (or y): it is commensurate ($\delta=1/4$) up to $y=0.25$, and becomes incommensurate for $y=0.3$, although the CO-OO order is still long ranged. It remains incommensurate for $y \geqslant 0.4$ (short-range CO-OO order). The variation of the magnetic, and electrical properties of ECSMO are summarized in the bottom panel of Fig. 3. T^* marks the appearance of diffuse superlattice spots in the EDPs (i.e., CO-OO correlation),[15] while T_g is the SG phase transition temperature, obtained from the dynamical scaling of the $T_f(f)$ freezing data of $\chi(T,f)$.[6,10] In the case of the crystal with $y=0.4$, no true SG phase transition is found, albeit glassiness below $T_f \sim 40$ K. While $T_{CO\text{-}OO}$ varies greatly with r_A, T_N is relatively unchanged for all the crystals with long-range CO-OO order.

The schematic phase diagram presented in Fig. 3 can also be plotted as a function of σ^2. The resulting diagram is very

similar, as both r_A and σ^2 vary significantly with y. It hence makes sense to draw a global phase diagram in the planes of r_A and σ^2 to take into account the effects of the variation of both bandwidth and quenched disorder. Such a bandwidth-disorder phase diagram is drawn in Fig. 4, using the ac susceptibility, resistivity, and electron diffraction data, which were found to complement each other in the above. This phase diagram is reminiscent of the diagram obtained for the 3D perovskite case[2] in the small-bandwidth area (for larger W, FM is observed in the perovskite case). In both cases, the long-range CO-OO order is replaced by a short-range CE-glass state (SG state) in the presence of large quenched disorder.[6,10] However, the first-order-like transition between the CO-OO and CE-glass phases observed in the perovskite case[4] does not occur in the layered systems. As indicated by the ED results, the CO-OO correlation length continuously decreases as the quenched disorder increases. Since there is a clear covariation between the CO-OO correlation length and the size of the "superspins" involved in the SG state, the latter of which were determined by the dynamical scaling of the $\chi(T,f)$ data,[10,15] these groups of coherent spins may be viewed as broken pieces of the CO-OO FM zigzag chains of the CE-type structure.

To summarize, we have established the intrinsic bandwidth-disorder phase diagram of the half-doped layered manganites using high-quality single crystals. As in the perovskite case, the CE-glass state occupies a large area of the diagram. Many specimens were found to exhibit a long-range CO-OO, with a $T_{\text{CO-OO}}$ tunable around room temperature and above by the bandwidth and/or disorder. The macroscopic phase separation, or ferromagnetic phases, sometimes reported in studies on polycrystals is not observed. Remarkably, the present diagram is very similar to that of the narrow-bandwidth perovskites, in spite of the dimensionality difference. However, in the present 2D layered case, the gradual decrease of the CO-OO correlation length as a function of bandwidth or disorder occurs, instead of the first-order-like collapse observed in the 3D case.

*Present address: Department of Microelectronics and Applied Physics, Condensed Matter Physics Group (KMF), Royal Institute of Technology (KTH), Electrum 229, SE-164 40 Kista, Sweden. Electronic address: rmathieu@kth.se

[1] Y. Tokura and N. Nagaosa, Science **288**, 462 (2000).
[2] Y. Tomioka and Y. Tokura, Phys. Rev. B **70**, 014432 (2004).
[3] Z. Jirák, S. Krupicka, Z. Simsa, M. Dlouhá, and Z. Vratislav, J. Magn. Magn. Mater. **53**, 153 (1985).
[4] D. Akahoshi, M. Uchida, Y. Tomioka, T. Arima, Y. Matsui, and Y. Tokura, Phys. Rev. Lett. **90**, 177203 (2003).
[5] H. Aliaga, D. Magnoux, A. Moreo, D. Poilblanc, S. Yunoki, and E. Dagotto, Phys. Rev. B **68**, 104405 (2003).
[6] R. Mathieu, D. Akahoshi, A. Asamitsu, Y. Tomioka, and Y. Tokura, Phys. Rev. Lett. **93**, 227202 (2004).
[7] N. Takeshita, C. Terakura, D. Akahoshi, Y. Tokura, and H. Takagi, Phys. Rev. B **69**, 180405(R) (2004).
[8] B. J. Sternlieb, J. P. Hill, U. C. Wildgruber, G. M. Luke, B. Nachumi, Y. Moritomo, and Y. Tokura, Phys. Rev. Lett. **76**, 2169 (1996).
[9] M. Ibarra, R. Retoux, M. Hervieu, C. Autret, A. Maignan, C. Martin, and B. Raveau, J. Solid State Chem. **170**, 361 (2003).
[10] R. Mathieu, A. Asamitsu, Y. Kaneko, J. P. He, and Y. Tokura, Phys. Rev. B **72**, 014436 (2005).
[11] J. P. Attfield, Chem. Mater. **10**, 3239 (1998).
[12] Y. Moritomo, Y. Tomioka, A. Asamitsu, Y. Tokura, and Y. Matsui, Phys. Rev. B **51**, R3297 (1995).
[13] D. J. Huang *et al.* (unpublished).
[14] The broad peak at high T vanishes near R=Eu, which shows a sharp cusp at low T. The crystals with long-range CO-OO have no f-dependent $\chi'(T)$, and $\chi''(T)$ is negligible. On the other hand, the crystals with short-range CO-OO show some glassiness or well-defined SG phase transitions related to the sharp cusps in $\chi'(T)$.
[15] M. Uchida, R. Mathieu, J. P. He, Y. Kaneko, A. Asamitsu, R. Kumai, Y. Tomioka, Y. Matsui, and Y. Tokura, J. Phys. Soc. Jpn. **75**, 053602 (2006).
[16] These crystals adopt the *Pnma* structure, with nearly identical a and b lattice parameters; the tilting of the MnO_6 octahedra yields smaller Mn-O-Mn bond angles.